Published in the Proceedings of the 16th International Aluminum Alloys Conference (ICAA16) 2018
ISBN: 978-1-926872-41-4
by the Canadian Institute of Mining, Metallurgy & Petroleum

MODELING THE DYNAMIC MECHANICAL BEHAVIOUR AND TEXTURE EVOLUTION OF ADDITIVELY MANUFACTURED AlSi10Mg_200C

*Edward Cyr and Mohsen Mohammadi

Marine Additive Manufacturing Centre of Excellence (MAMCE)
University of New Brunswick, Fredericton, New Brunswick, Canada
*(*Corresponding author: ecyr@unb.ca)*

ABSTRACT

To date, several studies have been performed on the static mechanical properties of SLM-AlSi10Mg alloy. There have also been more recent studies on the relation between scan strategy, texture, and mechanical properties of SLM metals and composites. However, there is a huge knowledge gap in the available literature regarding texture and mechanical behavior of SLM-AlSi10Mg alloy under high strain rates. Therefore, in this study, dynamic mechanical behavior of AlSi10Mg_200C alloy manufactured by DMLS technique was investigated at high strain rates ranging from 900/s to 1700/s using Split Hopkinson Pressure Bar. Texture using X-ray diffraction technique of the initial samples were measured. The yield strength, peak flow stress, and ductility increased in all samples with increase of strain rate. TEM studies have also revealed evidence of continuous dynamic recrystallization in grains after 900/s–1700/s strain-rate tests. A Taylor polycrystal crystal plasticity constitutive model was then developed to capture and predict the texture evolution and mechanical response under dynamic loading, using plastic work as a critical parameter for the onset of recrystallization.

KEYWORDS

Additive manufacturing, AlSi10Mg_200C, Crystal plasticity, DMLS, Texture

INTRODUCTION

Additive manufacturing (AM) powder techniques are among the fastest advancing breakthroughs in manufacturing in recent years, defined by a bottom-up layer by layer process of joining with energy input from lasers or electron beam (Herzog et al., 2016; Gibson et al., 2015). Among alloys fabricated by SLM, AlSi10Mg is of high interest to industry and academia due to its low density, high specific strength and excellent corrosion resistance, making this alloy a viable contender for aerospace, automotive, and marine applications. Circumstances such as car crash or bird aircraft strike hazards subject potential additively manufactured AlSi10Mg parts to impact loadings. This drives an interest in understanding and predicting dynamic behaviour of these alloys.

AlSi10Mg is the AM counterpart of A360 die-cast aluminum, which possess hypoeutectic microstructure (Li et al., 2015). Up to the present time, many studies have presented the mechanical properties of SLM-AlSi10Mg alloy. The mechanical properties and microstructure of AlSi10Mg produced by selective laser melting (SLM) or DMLS techniques can be controlled using different parameters, such as feedstock powder (Asgari et al., 2017), and process parameters (Olakanmi et al., 2015). The microstructure and mechanical properties of AlSi10Mg can also be controlled using post heat treatment after SLM process Li et al., 2016). The mechanical properties of SLM-AlSi10Mg are sensitive to strain rate and can both change under quasi-static (Rosenthal et al., 2017) and high strain rates (Asgari et al., 2018). However, a significant knowledge gap in available literature regarding modeling these behaviours, and especially micromechanical modeling of dynamic behaviour.

In general, dynamic deformation behavior of metallic alloys is a complex phenomenon, and is largely characterized by competition between strain hardening and thermal softening. Thermal softening can be further split into dynamic recovery, which involves the remobilization and annihilation of dislocations, and dynamic recrystallization, where nucleation and growth of new grains dominates the mechanical response (Solhjoo, 2014). Although derived from varying physical theories, the models of flow stress curves available in literature are functions of strain, strain rate, and temperature. Work hardening and dynamic recovery compete to control the flow stress up to a maximum stress. However dynamic recrystallization (DRX) begins before this maximum. Determination of this DRX initiation has been studied extensively, however all attempts to model such behaviour have either neglected material texture, or required complex phase-field or crystal plasticity finite element software (Najafizadeg & Jonas, 2006; Ebrahimi & Soljhou, 2007; Solhjoo, 2010). This study is the first to attempt to model such a behaviour using a simple crystal plasticity Taylor polycrystal averaging framework.

Of particular interest in this paper is the Direct Metal Laser Sintering (DMLS) of AlSi10Mg_200C and the resultant material/microstructure behaviour under high strain rates. Metal powder was provided by EOS of North America, with chemical composition as in (Mohammadi & Asgari, 2017). Cylindrical samples were printed using a 400W EOS M290 printer with the print bed held at 200ºC. As-printed samples were then machined to ASTM standard dimensions and strained by a Split Hopkinson Pressure Bar and stress-strain data was recorded.

CRYSTAL PLASTICITY MODELING

Work Hardening Flow Stress

The general crystal plasticity formulation used in this study follows the constitutive framework presented in (Cyr, 2017) with the constitutive law

$$\overset{\nabla}{\sigma} = \mathcal{L}D - \dot{\sigma}_0 - \sigma trD, \tag{1}$$

where $\overset{\nabla}{\sigma}$ is the Jaumann rate of Cauchy stress, $\mathcal{L}$ is the fourth rank tensor of elastic moduli, D is the total strain rate, and $\dot{\sigma}_0$ is the slip-rate dependent viscoplastic stress rate.

The general form of the flow stress curves is a hyperbolic tangent, where post-yield, the materials exhibits an almost linear hardening up to a first peak, then a secondary hardening where recovery and recrystallization occurs. Work hardening is therefore modeled using the Chang and Asaro (1981) single-slip hardening relationship shown in equation (2), where material hardening h_α evolves with accumulated shear strain γ.

$$h_\alpha = h_s + (h_0 - h_s)\,\mathrm{sech}^2\left(\frac{h_0 - h_s}{\tau_s - \tau_0}\gamma\right) \tag{2}$$

were h_0 and h_s are the initial and saturated hardening rates, respectively, and τ_0 and τ_s are the initial and saturated slip strength, respectively. The accumulated shear γ is determined by

$$\gamma = \int_0^t \sum_\alpha \dot{\gamma}^\alpha dt, \tag{3}$$

where slip system shear rate $\dot{\gamma}^\alpha$ is determined using the power law relation

$$\dot{\gamma}^\alpha = \dot{\gamma}_0 \mathrm{sgn}(\tau_s^\alpha)\left|\frac{\tau_s^\alpha}{\tau_y}\right|^{1/m}. \tag{4}$$

Here, τ_s^α is the resolved shear stress on slip system α, as determined by the Schmid factor, m is the slip rate exponent, and τ_y is the current slip strength—which can be determined simply from equation (2) if it is assumed that there is no latent hardening—found as:

$$\tau_y = \int_0^t \sum_\alpha h_\alpha\, \dot{\gamma}^\alpha\, dt. \tag{5}$$

Continuous Dynamic Recrystallization

Observations under transmission electron microscope (TEM) reveal that samples did not undergo conventional discrete dynamic recrystallization common in low stacking fault energy materials, where nuclei grow through the material leaving behind a relatively dislocation free grain in its wake. Instead, the initial entanglement of dislocations became organized into a strong cellular structure, similar to low angle grain boundaries, with a completely dislocation free cell interior (Hadadzadeh et al., 2018). These incredibly dense dislocation cell walls effectively refine the grain size, however TEM analysis concluded that the grains did not develop new crystal orientations. This phenomenon has been observed previously in wrought Al-Si-Mg alloys systems, e.g. (Lee et al., 2016) and Al-Li alloys, e.g. (Gurao et al., 2013) and is coined continuous dynamic recrystallization, or continuous recrystallization (CRX). In the CRX mechanism, new grains are not formed by nucleation and growth due to the high efficiency of dynamic recovery (DRV) due in part to high stacking fault energy. During CRX, subgrains develop as dislocations group to form low angle boundaries within the grain, and subsequently evolve to high angle grain boundaries as strain increases, with dislocation-free cell interiors.

In general, during hot deformation processing or dynamic loading, when the strain exceeds a critical value continuous recrystallization initiates driven by the removal of dislocations. Up to the peak stress, work hardening and dislocation density are increasing to a critical microstructural condition. This occurs at different rates in varying grains due to their crystal orientation and amount of slip that accumulates. Upon the peak stress, in the case of CRX, dislocation cell walls have formed and intense recovery of dislocations within these dislocation cells become dislocation free. From a modeling perspective, the crystal has been rapidly removed of significant dislocation content, but the yield and post CRX hardening has increased due to ‘grain size’ refinement. Grain size is in single quotations, because the parent grains are not changing size or orientation, rather is the intensity of the subgrain boundaries that are acting as grain size refinement.

Critical Strain

Critical stress/strain determination for recrystallization has been studied extensively, e.g. (Najafizadeg & Jonas, 2006; Ebrahimi & Soljhou, 2007; Solhjoo, 2010, 2014). In bulk material modeling, the critical stress/strain for the onset of DRX has been identified mathematically as the inflection point in the strain hardening rate $\theta = d\sigma/d\varepsilon$ *versus* flow stress σ curve. However, Poliak and Jonas concluded that this method based on energetic considerations was not sufficient (Poliak & Jonas, 1996). Additionally, macro-models are empirical in nature, and must rely on Avrami-type relations to account for recrystallization. In a crystal plasticity framework, this has been solved by using cellular automata algorithms to predict nucleation and growth within individual crystals based on the Nye tensor and crystal misorientations (Popova et al., 2015). However, for CRX, determination of a nucleus, and by extension its crystallographic orientation is not required. Thus, an energetic consideration within each crystal may provide a suitable initiation for the observed recrystallization in the AlSi10Mg_200C dynamic tests. Upon this critical condition, the flow stress of the recrystallized grain drops substantially, and then resumes work hardening. The contribution of all crystals in a polycrystal averaging scheme would lead to the observed high-strain rate behaviour of the bulk material, where texture and not only strain rate affects the rate at which the material recrystallizes.

The proposed criterion for recrystallization initiation is for a single crystal basis, and is presented mathematically by the amount of plastic work $W(t)$ at time t, i.e.

$$W(t) = \int_0^t \sum_{\alpha} \tau^{\alpha} \dot{\gamma}^{\alpha} \, dt, \tag{6}$$

where τ^{α} and $\dot{\gamma}^{\alpha}$ are the resolved stress and shear rate on slip system α, respectively. At a critical value W_c the crystal flow stress and crystal slip strength decreases, and dislocation density represented by the accumulated slip also decreases by some factor f_{crx} where $0 < f_{CRX} < 1$ represents the degree of recrystallization taken place. The rapidity of this transformation is assumed to be nearly instantaneous within the crystal. Work hardening of the recrystallized grains then resumes from this new state.

EXPERIMENTAL PROCEDURE

Material and DMLS Process

This study used experimental samples produced congruously to the study presented by Asgari et al. (2018), where vertical samples of AlSi10Mg were printed using an EOS M290 machine located at Additive Metal Manufacturing (AMM) in Concord, ON, Canada. The ‘dash’ 200C designation informs that the bed temperature during the print process was held at 200ºC to reduce thermal stresses. Figure 1 shows a representation of the print orientation, the printed vertical bars (grey) and the machined compression specimens (blue).

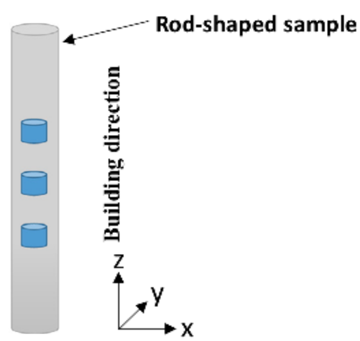

Figure 1. Print orientation for vertical compression samples.

High Strain Rate Test

This study is focused on the shock loading behaviour, which was investigated using a Split Hopkinson Pressure Bar (SHPB) at strain rates of 900/s, 1200/s, and 1700/s. All shock loading samples were machined from vertical bars, as shown above, with dimensions of 10.5 mm high, and 9.5 mm in diameter. Details regarding the shock loading test and related equations can be found in Tiamiyu et al. (2015). Presented experimental results are the averaged curves of three repeated tests.

Texture

Undeformed texture measurements were completed by sectioned samples along the compression direction. Using a Bruker D8 discover diffractometer with Co Kα radiation and VANTEC 500 area detector, the compression plane of the samples was subject to X-ray diffraction (XRD) with sample oscillation of 5 mm along the XY axis. The experimental {111}, {200}, and {220} pole figures are presented in Figure 2. Mild texture is evident in the as-built state, with mild Cube and rotated Goss intensities.

The simulated texture was generated using the open-source MTex software in Matlab and the XRD data measured for the samples. The same pole figures generated from the simulated texture is also presented in Figure 2, using 5000 crystal orientations to very closely match the measured texture.

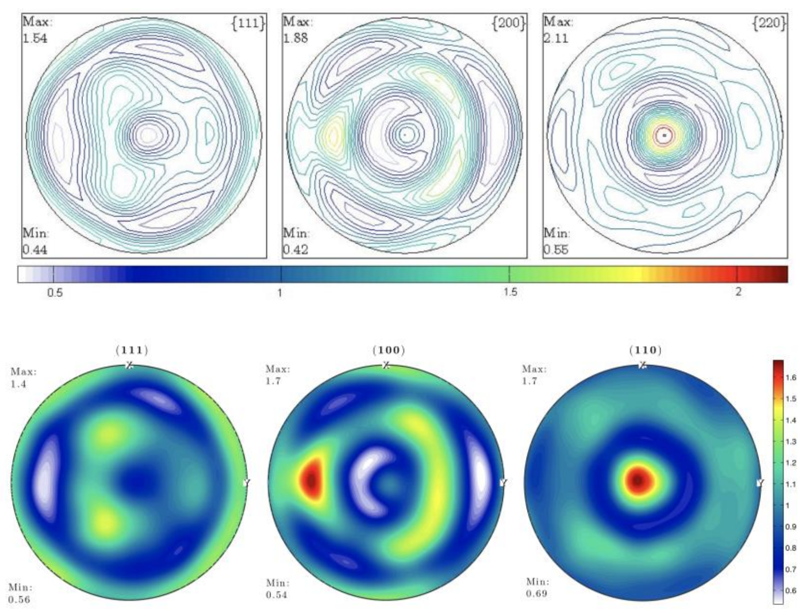

Figure 2. Experimental texture from XRD (top) and simulated texture using 5000 crystal orientations (bottom).

RESULTS AND DISCUSSION

Using equation (1) in a Taylor-type polycrystal averaging scheme, the flow stress was calculated for the three investigated shock loading strain rates and compared with experimental results. The comparison is illustrated in Figure 3(a). In all three instances, the simulated stress-strain is able to model the experimental stress-strain curve very will up to the second peak. The model does not consider the softening beyond the second peak, which is not quite understood and still under investigation. It should also be noted that the presented model does not include the effects of temperature increase during compression, and assumes that the effect of temperature increase is sufficiently captured in the evolution of critical plastic work during CRX.

The evolution of the critical plastic work W_c was assumed to be a function of the volume of crystals that have undergone CRX. The reasoning for this is that, a recrystallizing grain creates a local stress relaxation, thus lowering the stress locally and decreasing the likeliness of neighbour grains recrystallizing. Since the Taylor polycrystal averaging scheme does not account for neighbour grain interactions explicitly, and therefore neighbour grains do not experience a stress relaxation, a fractional increase in the critical plastic work can produce the same effect. The difficulty is determining this evolution of W_c as a function of volume fraction of CRX grains.

From the literature, it is known that recrystallization propagates through the material according to an Avrami-type growth (Maire et al., 2017), where the initial rate of recrystallization is low, then rapidly increases, then asymptotically decreases to zero as the volume fraction of CRX grains approaches 100%. Therefore, it follows that the critical parameter to determine the onset of CRX, in this case plastic work, should increase rapidly upon initial CRX, then reach a moderate steady state increase until a final rapid increase up to 100% volume fraction. This type of behaviour was represented perfectly by an inverse sine relationship, modified to include limits for minimum and maximum critical plastic work W_c^{min} and W_c^{max}, respectively.

$$W_c = \left(\frac{W_c^{max} + W_c^{min}}{2}\right) + \left(\frac{W_c^{max} - W_c^{min}}{\pi}\right)\sin^{-1}(2VF - 1) \tag{7}$$

The illustration of this evolution of W_c *versus* volume fraction (VF) of CRX grains (equation (7)) is also presented in Figure 3(b). The model finds that W_c^{min} and W_c^{max} both increase with increasing strain rate, as can be expected upon observation of stress-strain data where first and second peaks occur at increasingly higher strains as strain-rate increases. This inverse relationship between critical work for CRX initiation and strain rate also suggests that the CRX mechanism is diffusional, where higher strain rates do now allow sufficient time for diffusional processes therefore the barrier for activation has an apparent increase. This is also observed in analysis where temperature is decreased, resulting in an increased barrier to recrystallization (Solhjoo, 2014).

Lastly, Figure 3(c) shows the simulated results for volume fraction of CRX grains *versus* total strain. These predictions agree very well with the Avrami-type behaviour observed in continuous recrystallization experiments (Jonas et al., 2009), where the onset of recrystallization occurs at higher strains for increasing strain rate. Additionally, the recovery factors f_{crx} for the 900/s, 1200/s, and 1700/s strain rates were found to be 0.85, 0.84, and 0.60, respectively.

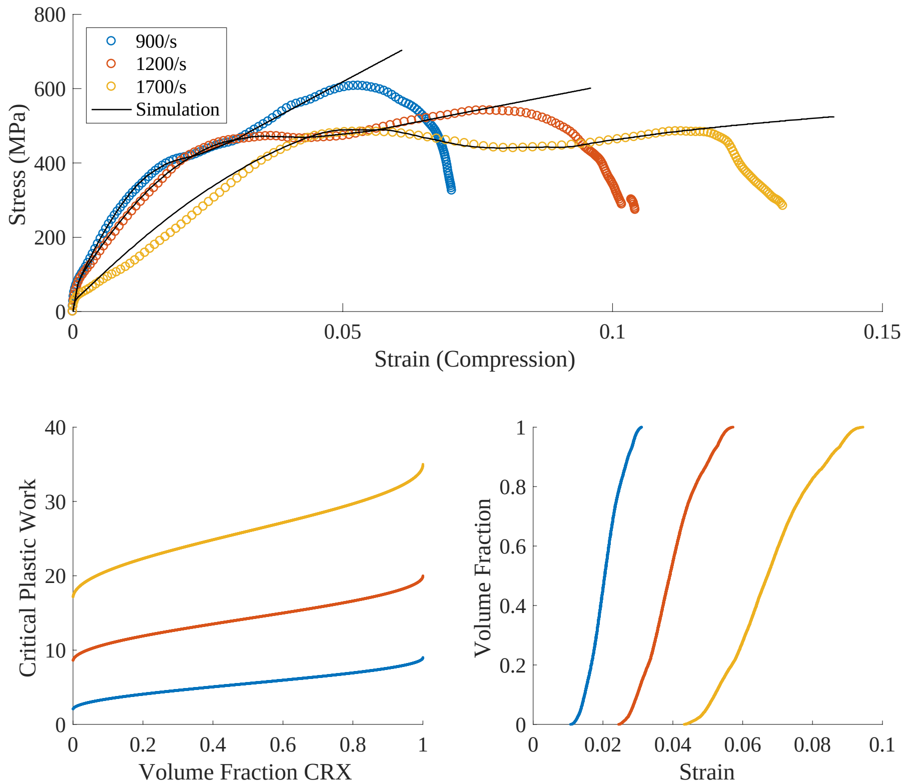

Figure 3. Logarithmic stress-strain data and corresponding simulation results (top), as well as critical plastic work evolution (bottom left), and volume fraction of CRX crystals vs. strain (bottom right).

CONCLUSIONS

A new and simple microstructure-based approach for modeling continuous recrystallization (CRX) using a Taylor polycrystal averaging scheme is developed and used to simulate the mechanical response and recrystallization during shock loading of AlSi10Mg-200C produced by DMLS. The model employs a critical plastic work criterion as a barrier for CRX initiation, which evolves with volume fraction of recrystallized grains according to an inverse sine relationship, and increases with increasing strain rate. The model is able to simulate accurately the CRX behaviour of the impacted AlSi10Mg and predicts the well-known Avrami-type relationship between volume fraction recrystallized grains and total strain.

REFERENCES

Aboulkhair, N. T., Maskery, I., Tuck, C., Ashcroft, I. & Everitt, N. M. (2016). On the formation of AlSi10Mg single tracks and layers in selective laser melting: Microstructure and nano-mechanical properties. *Journal of Materials Processing Technology*, *230*, pp.88–98.

AlMangour, B., Grzesiak, D. and Yang, J. M. (2016). Rapid fabrication of bulk-form TiB 2/316L stainless steel nanocomposites with novel reinforcement architecture and improved performance by selective laser melting. *Journal of Alloys and Compounds*, *680*, 480–493.

AlMangour, B., Grzesiak, D. and Yang, J. M. (2017). Scanning strategies for texture and anisotropy tailoring during selective laser melting of TiC/316L stainless steel nanocomposites. *Journal of Alloys and Compounds*, *728*, 424–435.

Asgari, H., Baxter, C., Hosseinkhani, K. & Mohammadi, M. (2017). On microstructure and mechanical properties of additively manufactured AlSi10Mg_200C using recycled powder. *Materials Science and Engineering A*, *707*, 148–158.

Asgari, H., Odeshi, A., Hosseinkhani, K. & Mohammadi, M. (2018). On dynamic mechanical behavior of additively manufactured AlSi10Mg_200C. *Materials Letters*, *211*, 187–190.

Chang Y. W., & Asaro R. J. (1981). An experimental study of shear localization in aluminum-copper single crystals, *Acta Metallurgica, 29*, 241–57.

Cyr, E., 2017. A New Crystal Plasticity Formulation to Simulate Large-Strain Plasticity of Polycrystalline Metals at Elevated Temperatures (Thesis). University of Waterloo, Waterloo, Canada.

Ebrahimi, R. and Solhjou, S. (2007). Characteristic points of stress-strain curve at high temperature.

Geiger, F., Kunze, K. & Etter, T. (2016). Tailoring the texture of IN738LC processed by selective laser melting (SLM) by specific scanning strategies. *Materials Science and Engineering A*, *661*, 240–246.

Gibson, I., Rosen, D. & Stucker, B. (2015). Design for additive manufacturing. In *Additive Manufacturing Technologies* (pp. 399-435). Springer New York.

Gurao, N. P., Adesola, A. O., Odeshi, A. G. & Szpunar, J. A. (2013). On the evolution of heterogeneous microstructure and microtexture in impacted aluminum–lithium alloy. *Journal of Alloys and Compounds*, *578*, 183–187.

Hadadzadeh, A., Amirkhiz, B. S., Li, J., & Odeshi, A. (2018). Deformation Mechanism in Impacted Additively Manufactured AlSi10Mg_200C, *Materials Science and Engineering A*, Submitted.

Herzog, D., Seyda, V., Wycisk, E. & Emmelmann, C. (2016). Additive manufacturing of metals. *Acta Materialia*, *117*, 371–392.

Jonas, J. J., Quelennec, X., Jiang, L., & Martin, É. (2009). The Avrami kinetics of dynamic recrystallization. *Acta materialia*, *57*(9), 2748–2756.

Kudzal, A., McWilliams, B., Hofmeister, C., Kellogg, F., Yu, J., Taggart-Scarff, J. & Liang, J. (2017). Effect of scan pattern on the microstructure and mechanical properties of powder bed fusion additive manufactured 17-4 stainless steel. *Materials & Design*, *133*, 205–215.

Lee, J. W., Son, K. T., Jung, T. K., Yoon, Y. O., Kim, S. K., Choi, H. J. & Hyun, S. K. (2016). Continuous dynamic recrystallization behavior and kinetics of Al–Mg–Si alloy modified with CaO-added Mg. *Materials Science and Engineering A*, *673*, 648–659.

Li, W., Li, S., Liu, J., Zhang, A., Zhou, Y., Wei, Q., Yan, C. & Shi, Y. (2016). Effect of heat treatment on AlSi10Mg alloy fabricated by selective laser melting: Microstructure evolution, mechanical properties and fracture mechanism. *Materials Science and Engineering A*, *663*, 116–125.

Li, X. P., Wang, X. J., Saunders, M., Suvorova, A., Zhang, L. C., Liu, Y. J., Fang, M. H., Huang, Z. H. & Sercombe, T. B. (2015). A selective laser melting and solution heat treatment refined Al–12Si alloy with a controllable ultrafine eutectic microstructure and 25% tensile ductility. *Acta Materialia*, *95*, 74–82.

Maire, L., Scholtes, B., Moussa, C., Bozzolo, N., Muñoz, D. P., Settefrati, A., & Bernacki, M. (2017). Modeling of dynamic and post-dynamic recrystallization by coupling a full field approach to phenomenological laws. *Materials & Design*, *133*, 498–519.

Mohammadi, M. and Asgari, H., 2017. Achieving low surface roughness AlSi10Mg_200C parts using direct metal laser sintering. *Additive Manufacturing*.

Najafizadeh, A. & Jonas, J. J. (2006). Predicting the critical stress for initiation of dynamic recrystallization. *ISIJ international*, *46*(11), 1679–1684.

Olakanmi, E. O. T., Cochrane, R. F. & Dalgarno, K. W. (2015). A review on selective laser sintering/melting (SLS/SLM) of aluminium alloy powders: Processing, microstructure, and properties. *Progress in Materials Science*, *74*, 401–477.

Poliak, E. I. & Jonas, J. J. (1996). A one-parameter approach to determining the critical conditions for the initiation of dynamic recrystallization. *Acta Materialia*, *44*(1), 127–136.

Popova, E., Staraselski, Y., Brahme, A., Mishra, R. K. & Inal, K. (2015). Coupled crystal plasticity–Probabilistic cellular automata approach to model dynamic recrystallization in magnesium alloys. *International Journal of Plasticity*, *66*, 85–102.

Rosenthal, I., Stern, A. & Frage, N., 2017. Strain rate sensitivity and fracture mechanism of AlSi10Mg parts produced by Selective Laser Melting. *Materials Science and Engineering A*, *682*, 509–517.

Solhjoo, S. (2010). Determination of critical strain for initiation of dynamic recrystallization. *Materials & Design*, *31*(3), 1360–1364.

Solhjoo, S. (2014). Determination of flow stress and the critical strain for the onset of dynamic recrystallization using a hyperbolic tangent function. *Materials & Design*, *54*, 390–393.

Tiamiyu, A. A., Basu, R., Odeshi. A. G., & Szpunar, J. A. (2015). Plastic deformation in relation to microstructure and texture evolution in AA 2017-T451 and AA 2624-T351 aluminum alloys under dynamic impact loading, *Materials Science and Engineering A, 636*, 379–388